Research Report Series 07/2025

St Michael's Church, Workington, Cumbria

Radiocarbon Dating and Chronological Modelling

Peter Marshall, Christopher Bronk Ramsey, Elaine Dunbar and John Zant

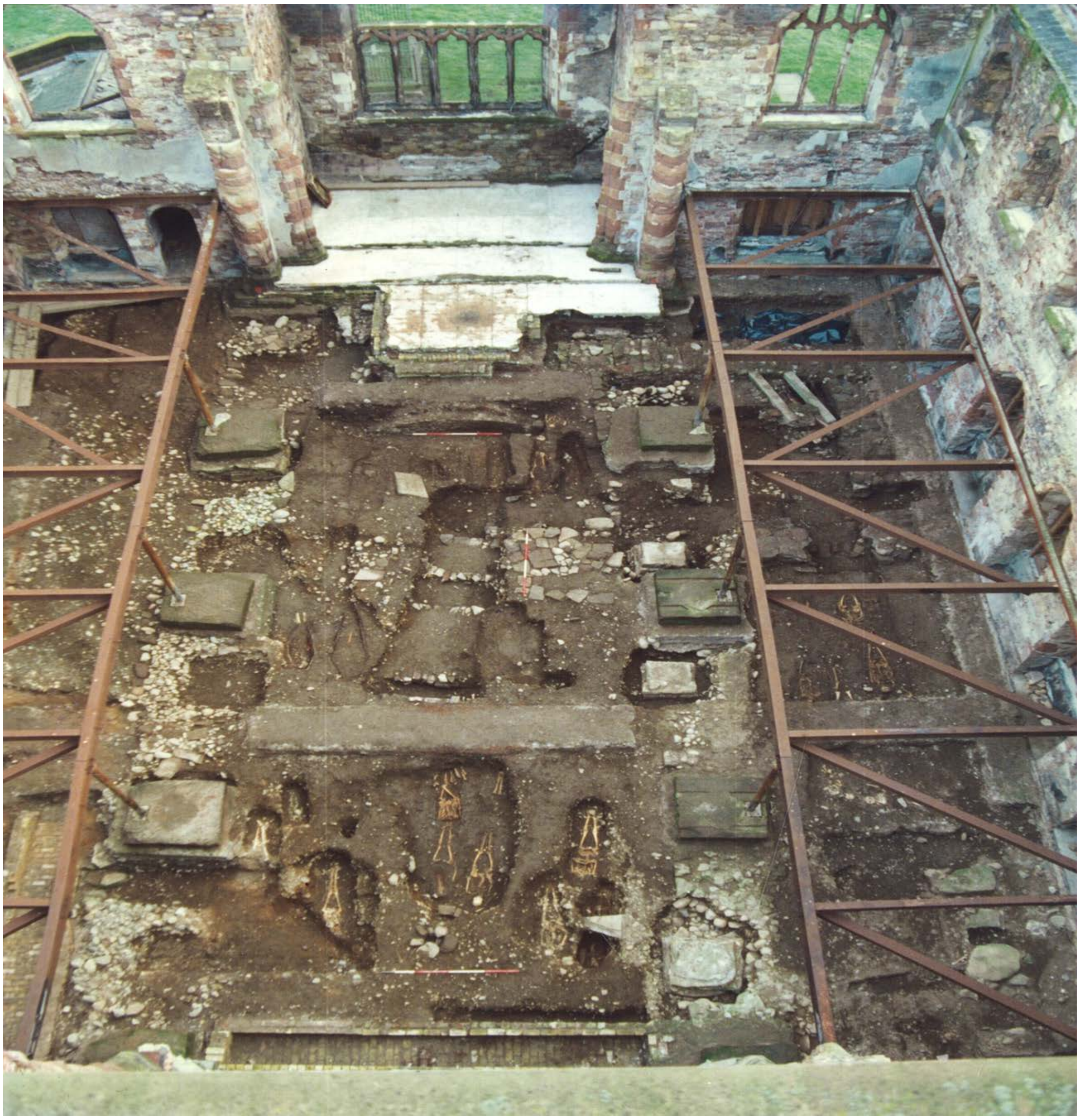

Scientific Dating

St Michael's Church, Workington, Cumbria

Radiocarbon Dating and Chronological Modelling

Peter Marshall, Christopher Bronk Ramsey, Elaine Dunbar and John Zant

NGR: NX 9975 2895

Print: ISSN 2398-3841
Online: ISSN 2059-4453

Summary

This report contains details of the radiocarbon and stable isotope measurements obtained from samples of human bone from St Michael's Church, Workington. Details of the assessment of collagen preservation are provided, and the chronological model previously published has been re-run using the currently internationally accepted radiocarbon calibration curve for the northern hemisphere (IntCal20). The posssibilty of diet-induced radiocarbon offset in the human skeleton for the site is considered. This provides a framework for the burial activity at the site that is very similar to that previously published.

Contributors

Peter Marshall, Christopher Bronk Ramsey, Elaine Dunbar and John Zant

Acknowledgements

Thanks to Helen Webb and Mark Gibson for help with sampling the human bones and to Alex Bayliss, Sue Stallibrass and Stephen Rowland for comments on early drafts of this report.

Front cover image

The interior of the church during the excavations (© Oxford Archaeology)

Archive location

The human remains are interred in the crypt of St Michael's Church, and the project archive, comprising all artefacts, and digital and paper records, is in the ownership of the Parochial Church Council.

Historic environment record

Cumbria Historic Environment Record, Cumbria County Council, County Offices, Kendal, Cumbria, LA9 4RQ

Date of research

2013–2017 and 2025

Contact details

Historic England, Cannon Bridge House, 25 Dowgate Hill, London, EC4R 2YA. 020 7973 3700. customers@HistoricEngland.org.uk

Peter Marshall Historic England, Cannon Bridge House, 25 Dowgate Hill, London EC4R 2YA, UK. pete.chronologies@googlemail.com

Christopher Bronk Ramsey, Oxford Radiocarbon Accelerator Unit, Dyson Perrins Building, South Parks Road, Oxford OX1 3QY. christopher.ramsey@arch.ox.ac.uk

Elaine Dunbar, Scottish Universities Environmental Research Centre, Scottish Enterprise Technology Park, Rankine Avenue, East Kilbride G75 0QF. elaine.dunbar@glasgow.ac.uk

John Zant, Oxford Archaeology North, Mill 3, Moor Lane Mills, Moor Lane, Lancaster LA1 1QD. john.zant@oxfordarch.co.uk

Contents

Illustrations

Tables

Introduction

This document is a technical archive report on the radiocarbon dating and chronological modelling of samples from human burials excavated at St Michael's Church, Workington, Cumbria (Fig. 1). A synthesis of the radiocarbon dating programme (Marshall et al. 2019) is included in the publication that offers full details on the excavations and post-excavation analysis (Zant and Parsons 2019).

A summary of the main periods of activity at St Michael's Church is outlined in Table 1.

Table 1. Periods of activity at St Michael's Church, Workington.

Phase	Description
1	Evidence for possible Roman activity provided by a few residual artefacts.
2a	A north-east/south-west-aligned ditch, pre-dating all other recorded features and deposits on the site, possibly enclosing the promontory on which the church site appears to have been located. Not closely dated but may not long pre-date Phase 2b.
2b	A group of at least 40 human burials, mostly aligned north-west/south-east, referencing the Phase 2a ditch. All but two of the graves lay either within/over the ditch, or immediately to the south-east, outside the possible promontory enclosure. A few of the sculptural fragments recovered from the St Michael's site may be contemporary with this phase.
3a	Evidence for continued (or renewed?) activity, including burial, during the first half of the tenth century, as indicated by the recovery of fragments of hogback grave markers and a late ninth- to early tenth-century gold ring, all residual or unstratified.
3b	A group of at least 18 east/west-aligned burials, the majority interred in stone-lined cists, located immediately outside the south wall of the later stone church. The cemetery may have been associated with an otherwise unattested (?wooden) church on the site. Much of the pre-Norman stone sculpture from the site may have been associated with this phase.
4	The earliest phase of the medieval stone church, comprising the nave, chancel, and (probably) tower. None of the recorded burials could be attributed to this period, but the great majority are not closely datable and there is no reason to suppose that a graveyard did not exist at this time.
5	Later additions to the medieval church, including the south door and its associated porch, insertion of the north door and construction of the Curwen burial vault, and continuation of burial within the church and churchyard.
6	Demolition of the medieval church and its reconstruction, AD 1770-2. Continuation of burial within the church and churchyard up to the mid–late-nineteenth century.
7	Church destroyed by fire, AD 1887 and subsequently rebuilt (consecrated in AD 1890). No further burials after this date.
8	Church damaged by fire, AD 1994 and subsequently rebuilt (consecrated in AD 2001).

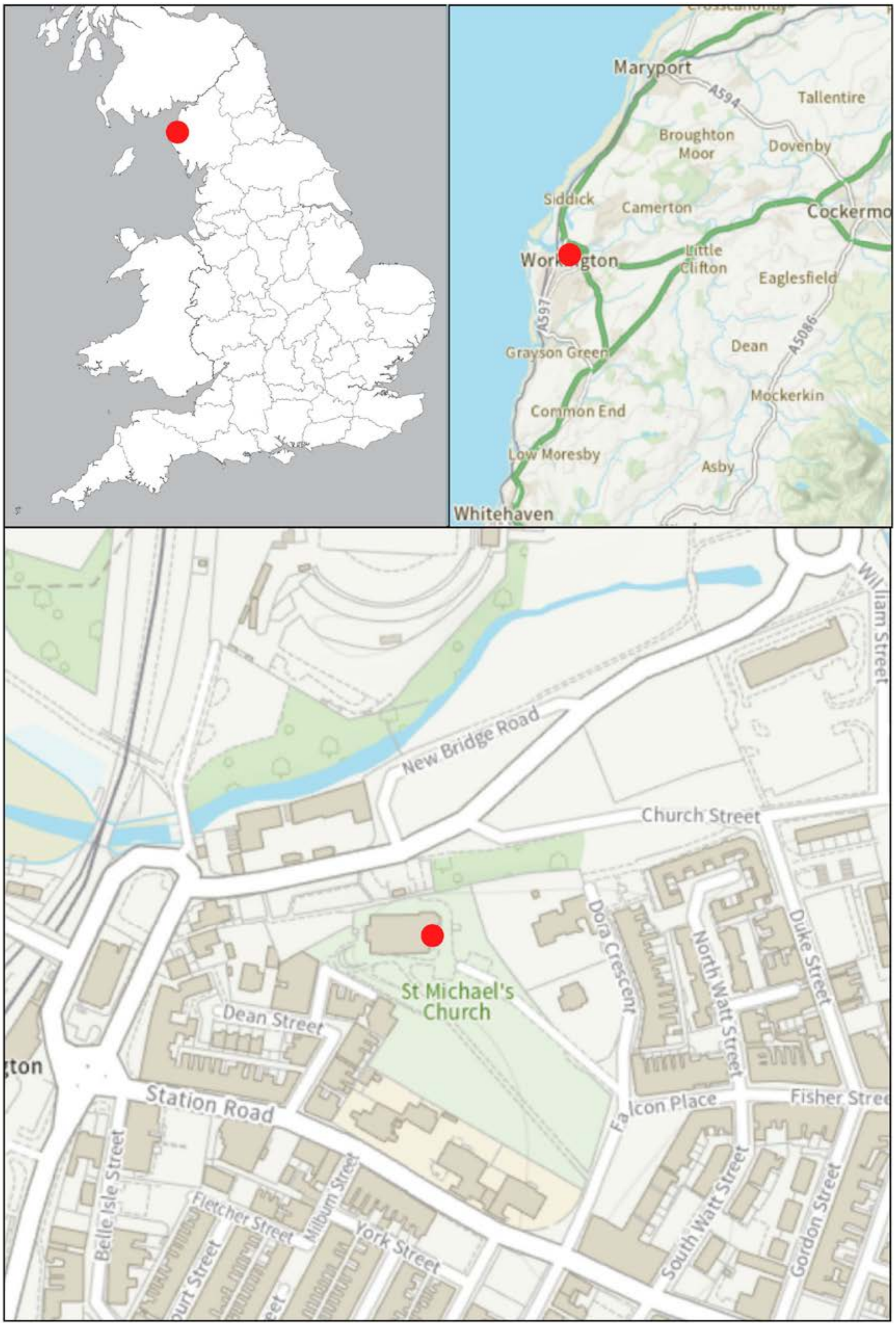

Figure 1. The location of St Michael's Church, Workington, Cumbria. Scale: top-right 1:200,000; bottom 1:2500. [© Crown Copyright and database right 2025. All rights reserved. Ordnance Survey Licence number 100024900]

The chronological modelling described in this report has been undertaken with the most recent revision of the radiocarbon calibration curve, IntCal20 (Reimer et al. 2020). IntCal20 includes more than five times as many measurements on known-age tree-rings from the period covered by burials from St Michael's Church (Bayliss et al. 2020) than previous iterations of the calibration curve (e.g. Reimer et al. 2013). This has the effect of revealing more structure in the changes in radiocarbon through time (Fig. 2) and, although these changes are modest in scale, they can shift modelled posterior distributions by several decades.

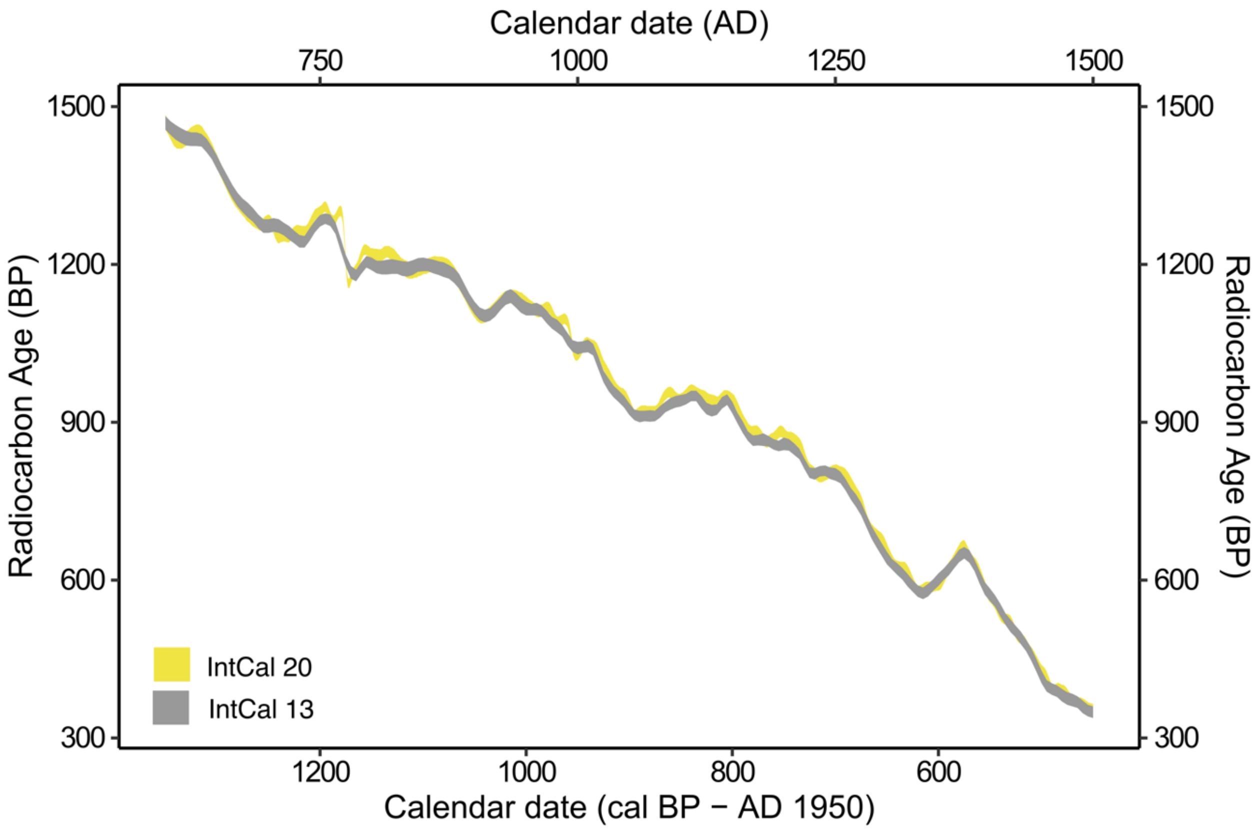

Figure 2. IntCal20 (yellow) and IntCal13 (grey) radiocarbon calibration curves (AD 600–AD 1500).

Consequently, in some instances, there will be small differences between the posterior density estimates for the dates of burials and other parameters reported below and those previously published (Zant and Parsons (2019). These changes, however, do not change the significance of the overall chronology.

We have also taken the opportunity to estimate statistically the potential for diet-induced radiocarbon offsets, which might have implications for the date of the radiocarbon dated individuals (Bayliss and Marshall 2022, §1.6), using a proportional isotopic mixing model to estimate the caloric contribution from potential food groups. An isotopic mixing model is an analytical model that allows the relative contribution of different food sources to the diets of an individual to be determined, based on the isotopic compositions of both the consumer and their dietary sources.

Objectives

The programme of radiocarbon dating and chronological modelling was designed to answer several specific questions relating to the sequence of burial at St Michael's Church and to provide:

- formal estimates of the date and duration of activity associated with the pre-Norman inhumation cemetery and early medieval cemetery;
- a *terminus post quem* for the construction of the medieval church (given the vast majority of the early medieval cemetery is stratigraphically earlier);
- a formal estimate for of the currency of cist-lined graves.

Sampling

Given the sand and gravel ridge on which the site is located and the likelihood of post-depositional diagenetic loss of bone collagen (Collins et al. 2002), a pre-screening programme was undertaken to determine whether bone samples suitable for radiocarbon dating survived on the site. The %N content of whole bone has been shown by Brock et al. (2010) to have an 84% probability of correctly predicting that a bone is suitable for dating (when %N is greater than 0.76%).

Samples from 75 skeletons were submitted for percentage nitrogen (%N) measurements to the Oxford Radiocarbon Accelerator Unit (ORAU). The results (Table 2) indicate that 81% of bones sampled were suitable for radiocarbon dating.

Sample selection was undertaken from this pool of viable potential samples using the iterative process for implementing Bayesian chronological modelling on archaeological sites outlined in Bayliss and Marshall (2022, §3). At St Michael's Church, we aimed to maximise the number of stratigraphic relationships between dated deposits included in the model. This relative sequence provides strong constraints on the model but, as stratigraphy provides a relative sequence of excavated deposits and radiocarbon dating provides dates for samples, it is essential to ensure that the sampled material is contemporary with its context and that it was in equilibrium with the atmosphere at the time the deposit was formed. As all the samples from St Michael's Church are from articulated skeletons, the corpses clearly went into the graves shortly after the sampled individual died. The sources of carbon in the human bone is more uncertain.

Table 2. St Michael's Church %N results (samples that have %N greater than 0.76% = Pass).

Skeleton	Element sampled	%N	Pass/Fail
Sk47	Left femur	1.2476	Pass
Sk123	Right femur	1.0823	Pass
Sk130	Left humerus	0.2916	Fail
Sk141	Right femur	1.9429	Pass
Sk159	Left tibia	1.4257	Pass
Sk166	Femur	0.6405	Fail
Sk168	Left tibia	0.8942	Pass
Sk172	Femur	0.3388	Fail
Sk174	Femoral shaft	1.6562	Pass
Sk179	Skull	0.3796	Fail
Sk191	Right femur	0.6796	Fail
Sk193	Left femur	1.4474	Pass
Sk196	Right humerus	0.9736	Pass
Sk200	Left femur	1.7808	Pass
Sk202	Left tibia	2.2361	Pass
Sk203	Right femur	0.4937	Fail
Sk204	Right femur	0.3958	Fail
Sk208	Right humerus	0.3821	Fail
Sk212	Left leg	0.3064	Fail
Sk217	Right femur	1.3710	Pass
Sk218	Humerus	1.7764	Pass
Sk219	Rib, left clavicle	1.7900	Pass
Sk223	Left femur	1.1941	Pass
Sk228	Right femur	1.1764	Pass
Sk237	Left femur	1.2366	Pass
Sk238	Left femur	0.4849	Fail
Sk239	Right femur	1.1090	Pass
Sk240	Left femur	0.9947	Pass
Sk241	Left femur	1.6789	Pass
Sk254	Left femur	1.6017	Pass
Sk255	Left femur	1.8591	Pass
Sk256	Left femur	1.6799	Pass
Sk259	Rib	2.1768	Pass
Sk261	Left femur	1.3651	Pass
Sk263	Left femur	1.3509	Pass
Sk264	Left tibia	1.9070	Pass

Skeleton	Element sampled	%N	Pass/Fail
Sk265	Left femur	1.7149	Pass
Sk266	Right humerus	0.3985	Fail
Sk267	Right humerus	0.9536	Pass
Sk268	Humerus fragment	0.3360	Fail
Sk281	Tibia	1.1668	Pass
Sk285	Left tibia	1.4151	Pass
Sk288	Right tibia	1.6249	Pass
Sk290	Skull fragment	1.7196	Pass
Sk291	Tibia fragment	1.2863	Pass
Sk292	Left femur	1.2258	Pass
Sk293	Right humerus	1.5252	Pass
Sk294	Right tibia	1.1746	Pass
Sk295	Left tibia	1.2685	Pass
Sk296	Right tibia	1.6374	Pass
Sk296b	Left temporal	1.1736	Pass
Sk297	Left tibia	2.2600	Pass
Sk298	Right femur	0.4010	Fail
Sk299	Left humerus	1.6163	Pass
Sk300	Right tibia	1.3051	Pass
Sk301	Right femur	1.0805	Pass
Sk303	Left tibia	1.6464	Pass
Sk304	Femur	0.5166	Fail
Sk305	Right femur	2.1589	Pass
Sk306	Right femur	1.3773	Pass
Sk307	-	1.3001	Pass
Sk351	Left humerus	2.1240	Pass
Sk352	Clavicle	0.9302	Pass
Sk353	Left tibia	2.3542	Pass
Sk354	Tibia	2.4250	Pass
Sk355	-	1.1443	Pass
Sk360	Tibia	1.6552	Pass
Sk361	Right humerus	2.0363	Pass
Sk362	Left tibia	1.5453	Pass
Sk363	Left tibia	0.8190	Pass
Sk364	Tibia	1.3374	Pass
Sk365	Humerus	2.0099	Pass
Sk366	Humerus shaft	2.0821	Pass

Skeleton	Element sampled	%N	Pass/Fail
Sk367	-	1.5371	Pass
Sk368	-	1.1591	Pass

Radiocarbon results

A total of 26 radiocarbon measurements are available for St Michael's Church (Table 3). The radiocarbon results are conventional radiocarbon ages, corrected for fractionation (Stuiver and Polach 1977; Table 3). Age calculation has been undertaken using $\delta^{13}C$ values measured by Accelerator Mass Spectrometry (AMS), except at the Scottish Universities Environmental Research Centre (SUERC) where the values obtained by Isotope Ratio mass Spectrometry (IRMS) were used. The quoted $\delta^{13}C$ values are those measured by IRMS as these more accurately reflect the natural isotopic composition of the sampled material.

At the Scottish Universities Environmental Research Centre (SUERC-), samples were pretreated and dated as described by Dunbar et al. (2016). The gelatin fraction of bone samples was extracted using a modified version of the method introduced by Longin (1971) before ultrafiltration. The samples were then converted to carbon dioxide in pre-cleaned sealed quartz tubes (Vandeputte et al. 1996), which was then graphitised as described by Slota et al. (1987) and measured by AMS using the SUERC SSAMS (Freeman et al. 2010; Naysmith et al. 2010).

The Oxford Radiocarbon Accelerator Unit (OxA-, OxA-X-) pretreated, gelatinised, and ultrafiltered bone samples following the methods outlined in Bronk Ramsey et al. (2004a). The samples were then converted to carbon dioxide, by combustion (Hedges et al. 1992), graphitised (Dee and Bronk Ramsey 2000) and dated using the HVEE AMS (Bronk Ramsey et al 2004b).

Table 3. St Michael's Church, radiocarbon and stable isotope results. Replicate measurements have been tested for statistical consistency and combined by taking a weighted mean before calibration as described by Ward and Wilson (1978; T′(5%)=3.8, v=1; except where stated).

Laboratory code	Sample reference, material & context	$\delta^{13}C_{IRMS}$ (‰)	$\delta^{15}N_{IRMS}$ (‰)	C:N	Radiocarbon age (BP)	*Posterior Density Estimate – cal AD (95% probability*)
Phase 2b						
OxA-X-2581-42	G166. Human bone, ?female, prime adult, femur from inhumation G166. G166 had probably been placed within a stratigraphically earlier ditch (975). G166 was cut by an east/west-aligned inhumation burial and had itself been dug through an earlier Phase 2 grave (G167). G167 was cut through an even earlier Phase 2 grave (G174).	−19.7±0.2	10.7±0.3	3.2	1150±23	*770–905 (86%)* or *915–955 (9%)*
OxA-29265	G174 sample A. Human bone, ??female, middle-adult, femoral shaft from inhumation G174, associated with two iron coffin fittings/hinges. G174 stratigraphically post-dated (and had probably been set within) backfilled ditch 975, and itself pre-dated three later inhumation burials of the same (pre-Norman) phase (G166, G167, and G172)	−20.3±0.2	11.2±0.3	3.3	1312±27	-
OxA-29266	G174 sample A. Replicate of OxA-29265	−20.3±0.2	11.3±0.3	3.3	1268±26	-
SUERC-49794	G174 sample B. Replicate of OxA-29265	−20.7±0.2	11.5±0.3	3.3	1275±26	-
G174	^{14}C: 1284±16 BP, T′=1.6, v=2; T′(5%)=6.0; $\delta^{13}C$ = −20.4±0.1‰, T′=2.7, v=2; T′(5%)=6.0; $\delta^{15}N$ = 11.4±0.2‰, T′=0.3, v=2; T′(5%)=6.0					*670–775*
SUERC-49804	G196. Human bone, ?female, mature adult, right humerus from inhumation G196. G196 appears to have been dug directly into the natural sandy gravel, to the south of ditch 975 and pre-dated a later inhumation burial of the same (pre-Norman) phase (G193). It is directly associated with diagnostic pre-Norman artefacts: a copper-alloy belt buckle and strap end set, a whetstone, an iron knife and an iron sickle.	−20.7±0.2	10.8±0.3	3.3	1213±28	*690–745 (18%)* or *770–885 (77%)*

Laboratory code	Sample reference, material & context	$\delta^{13}C_{IRMS}$ (‰)	$\delta^{15}N_{IRMS}$ (‰)	C:N	Radiocarbon age (BP)	*Posterior Density Estimate – cal AD (95% probability*)
SUERC-49796	G202. Human bone, young adult, left tibia from inhumation G202. G202 had probably been placed within a stratigraphically earlier ditch (975) and pre-dated a later inhumation burial of the same (pre-Norman) phase (G201).	−20.4±0.2	11.2±0.3	3.3	1407±26	*605–665*
OxA-29274	G218. Human bone, female, prime adult, humerus from inhumation G218. G218 was located south of early ditch 975 and cut a later inhumation burial of the same (pre-Norman) phase (G219). Its spatial position suggests the possibility that the bottom half of the grave had been cut by the foundation for the south chancel arch wall of the twelfth-century parish church	−19.8±0.2	10.3±0.3	3.3	1268±26	*665–780 (89%)* or *790–825 (6%)*
OxA-29273	G267. Human bone, ?,male, young adult, humerus from inhumation G267. G267 probably lay south of early ditch 975 and cut a later inhumation burial of the same (pre-Norman) phase (G268)	−19.4±0.2	11.2±0.3	3.3	1287±26	*665–775*
OxA-29271	G.281. Human bone, adult (>17 years), tibia from inhumation G281. G281 was located to the north of early ditch 975, one of only two of the excavated pre-Norman graves to have been situated north of this feature	−20.5±0.2	10.3±0.3	3.3	1248±26	*670–835 (92%)* or *850–875 (3%)*
Phase 3b						
SUERC-49800	G.141. Human bone, ?female, young-adult, right femur from inhumation G141. G141 was cut by the construction pit (385) for the font of the medieval parish church.	−21.0±0.2	10.7±0.3	3.3	1002±30	*990–1055 (92%)* or *1080–1095 (2%)* or *1105–1120 (1%)*
SUERC-49797	G168. Human bone, ?female, prime adult, left tibia from inhumation G168. G168 was an unlined burial located outside the north-east corner of the medieval parish church (north of the chancel) cut an earlier inhumation (G172).	−20.9±0.2	11.0±0.3	3.3	1057±30	*990–1040*

Laboratory code	Sample reference, material & context	$\delta^{13}C_{IRMS}$ (‰)	$\delta^{15}N_{IRMS}$ (‰)	C:N	Radiocarbon age (BP)	*Posterior Density Estimate – cal AD (95% probability)*
SUERC-53442	G193. Human bone, older-child, left femur from inhumation G193. G193 appears to have been dug into the natural sandy gravel, to the south of ditch 975. It cut an earlier inhumation burial (G196) of the same (pre-Norman) phase (Phase 2). G193 itself was stratigraphically earlier than the foundation for the south wall of the nave of the stone parish church, which may have been constructed in the early twelfth century	−20.1±0.2	12.1±0.3	3.3	903±30	*1024–1105*
OxA-29268	G256. Human bone, ?male, middle-adult, left femur from inhumation G256. Inhumation G256 was a stone-lined cist burial cut by the south wall of the nave of the medieval parish church, one of 11 such cists located in a restricted area adjacent to the south wall of the medieval nave, which are thought to relate to the earliest phase of the church cemetery	−20.1±0.2	9.5±0.3	3.4	1030±25	*995–1040*
OxA-29267	G300 – sample A. Human bone, male, prime-adult, right tibia from inhumation G300. Inhumation G300 was a stone-lined cist burial located adjacent to the south wall of the nave of the medieval parish church. The cist was unusual in that it appeared to contain two adult inhumations: a primary burial (G303) overlain by G300 itself. The cist cut an early burial, attributed to the pre-Norman phase (G305).	−20.3±0.2	9.5±0.3	3.3	993±27	-
SUERC-49795	G300 – sample B. Replicate of OxA--29267	−20.6±0.2	9.8±0.3	3.3	997±26	-
G300	^{14}C: 995±19 BP, T′=0.1; $\delta^{13}C$ = −20.5±0.15‰, T′=1.1; $\delta^{15}N$ = 9.7±0.2‰, T′=0.5					*1020–1051 (84%)* or *1083–1097 (4%)* or *1102–1123 (7%)*

Laboratory code	Sample reference, material & context	$\delta^{13}C_{IRMS}$ (‰)	$\delta^{15}N_{IRMS}$ (‰)	C:N	Radiocarbon age (BP)	*Posterior Density Estimate – cal AD (95% probability)*
SUERC-53443	G303. Human bone, ??male, middle-adult, left tibia from inhumation G303. G303 was a stone-lined cist burial located adjacent to the south wall of the nave of the medieval parish church. The cist was unusual in that it definitely contained two adult inhumations: a primary burial (G303 itself) overlain by a later skeleton (G300). The cist cut an earlier burial, attributed to Phase 2 (G305)	−20.7±0.2	10.1±0.3	3.2	977±30	*990–1055 (93%) or 1080–1100 (2%)*
SUERC-53444	G306. Human bone, mature adult, right femur from inhumation G306. G306 was a stone-lined cist burial located adjacent to the south wall of the nave of the medieval parish church, one of several cists of this kind found in a restricted area on the south side of the stone church	−20.8±0.2	11.1±0.3	3.3	969±30	*1017–1121*
OxA-30232	G307. Human bone, infant (1.5–12 months), humerus shaft from inhumation G307. G307 was a stone-lined cist burial located adjacent to the south wall of the nave of the medieval parish church	−19.6±0.2	12.8±0.3	3.1	1008±23	*995–1050*
OxA-29270	G360. Human bone, older child (7–9 years), tibia from inhumation G360. G360 was a stone-lined cist grave located immediately south of the medieval parish church	−20.7±0.2	9.9±0.3	3.4	971±26	*1018–1071 (85%)* or *1077–1124 (10%)*
OxA-30233	G361. Human bone, ?female, middle adult, right humerus from inhumation G361. G361 was a stone-lined cist burial located adjacent to the south wall of the nave of the medieval parish church	−20.3±0.2	10.6±0.3	3.1	948±23	*1024–1113*
Phase 5						

Laboratory code	Sample reference, material & context	$\delta^{13}C_{IRMS}$ (‰)	$\delta^{15}N_{IRMS}$ (‰)	C:N	Radiocarbon age (BP)	*Posterior Density Estimate – cal AD (95% probability)*
OxA-30378	G123 – sample A. Human bone, ?female, middle-adult, right femur from inhumation G123. G123 was an unlined, seemingly un-coffined inhumation burial located outside the north-east corner of the medieval stone church, north of the chancel. G123 was one of three graves in this area, located near each other, that had large cobbles placed either side of the head ('pillows')	−19.1±0.2	11.8±0.3	3.3	478±23	-
SUERC-53313	G123 – sample B. Replicate of OxA-30378	−19.7±0.2	12.0±0.3	3.2	492±19	-
G123	^{14}C: 486±15 BP, T′=0.2; $\delta^{13}C$ = −19.4±0.15‰, T′=4.5; $\delta^{15}N$ = 11.8±0.2‰, T′=0.0					*1417–1446*
SUERC-49799	G294. Human bone, young child (2–3 years), right tibia from inhumation G294. G294 may have been located within a stratigraphically earlier ditch (975). The foot of the grave was cut or overlain by the west wall of the south porch of the medieval church, itself probably a later (though possibly twelfth-century?) addition to the early twelfth-century fabric	−20.7±0.2	11.3±0.3	3.3	761±30	*1221–1279*
OxA-29272	G296. Human bone, male, adult (>17 years), right tibia from inhumation G296. G296 was an unlined grave located immediately south of the medieval parish church, and it post-dated three successive 'sub-phases' of inhumation burials (earliest to latest: G353, G354, G352)	−19.6±0.2	11.5±0.3	3.3	411±24	*1435–1496*
SUERC-49798	G353. Human bone, left femur from inhumation G353. G353 was a stone-lined cist grave located immediately south of the medieval parish church, one of 11 such cists located in a restricted area adjacent to the south wall of the medieval nave, which are thought to relate to the earliest phase of the church cemetery. It was cut by three successive 'sub-phases' of unlined inhumation burials (earliest to latest: G354, G352, G296)	−20.2±0.2	11.5±0.3	3.2	698±30	*1269–1312 (71%) or 1361–1389 (24%)*

Laboratory code	Sample reference, material & context	$\delta^{13}C_{IRMS}$ (‰)	$\delta^{15}N_{IRMS}$ (‰)	C:N	Radiocarbon age (BP)	*Posterior Density Estimate – cal AD (95% probability*)
OxA-29269	G363. Human bone, older child, left tibia from inhumation G363. G363 was an unlined grave located south of the medieval parish church. It was stratigraphically later than three other (unlined) inhumation burials (G364, G365, G366), and stratigraphically pre-dated another unlined inhumation (G362)	−20.1±0.2	10.2±0.3	3.3	590±25	*1304–1366 (71%) or 1382–1409 (24%)*

Quality assurance

Both facilities maintain continual programmes of quality assurance procedures, in addition to participation in international inter-comparison exercises (Scott et al. 2017).

Two pairs of replicates (G123; OxA-30378 and SUERC-53313, G300; OxA-29267 and SUERC-49795) and one set of triplicate measurements (G174; OxA-29265–6 and SUERC-49794) are available on samples that were divided and submitted for dating to both laboratories. In all cases the measurements are statistically consistent at the 5% significance level (Table 3) and their weighted mean therefore provides the best estimate of the radiocarbon age of the sampled individual (Ward and Wilson 1978).

Groups of carbon and nitrogen stable isotope ratios are also available on three individuals (G123; OxA-30378 and SUERC-53313, G300; OxA-29267 and SUERC-49795; G174; OxA-29265–6 and SUERC-49794). The three groups of nitrogen stable isotope ratios measurement are statistically consistent at the 5% significance level, while two of the groups of carbon stable isotope ratios measurement are statistically consistent at the 5% significance level (G174 and G300) and the third (G123) are statistically consistent at the 1% significance level —this reproducibility is within statistical expectation.

Diet-induced radiocarbon offsets?

Introduction

We undertook proportional diet profiling for the 22 dated individuals (Table 3) to determine the potential for diet-induced radiocarbon offsets (Bayliss and Marshall 2022), that might have implications for the chronology of the burials.

Background

Stable carbon and nitrogen isotopes are particularly useful for addressing ecological and social questions related to food consumption. This approach relies on detecting variations in isotopic ratios among different environments, organisms and their tissues. Isotopic results are expressed as δ values ($\delta^{13}C$ and $\delta^{15}N$) in parts per thousand or “per mil” (‰). The fractionation of carbon isotopes varies based on photosynthetic pathways and ecosystem types, allowing $\delta^{13}C$ (‰) values to discriminate between plants and their consumers (Peterson and Fry 1987) as well as between terrestrial, marine and freshwater ecosystems. Meanwhile, $\delta^{15}N$ (‰) values are influenced by climatic and environmental conditions and are primarily used as indicators of trophic levels (Heaton et al. 1986).

The stable isotope mixing model

We used the proportional mixing model ReSOURCES (Gross and Fernandes 2024) to estimate the caloric contribution of the 22 dated individuals from four potential food groups: terrestrial vegetation (cereals), terrestrial protein, marine fish and freshwater fish. Adapted from Scenario 2 described by Fernandes (2016), it is a routed and concentration-dependent model that takes account of the dietary contributions of protein and energy macronutrients, diet-to-consumer isotopic offsets, food macronutrient concentrations and corrections for isotopic differences between edible macronutrients and measured isotopic values in food remains (Fernandes et al. 2012, 2014, 2015).

Baseline isotopic values for food sources used in the modelling are detailed in Table 4. Both the sources and the baseline values were derived from Leggett et al. (2021). It is important to consider potential discrepancies between the isotopic values measured in food remains and those of the actual edible portions. To address this, we applied known offsets to estimate the isotopic values of food macronutrients (protein compared to lipids/carbohydrates) from the food sources. The corrected values for each food source given in Table 5 were derived by applying the following offset corrections to the values in Table 4, with uncertainties for macronutrient isotopic values rounded up to multiples of 0.5‰ (based on Fernandes et al. 2015; Soncin et al. 2021; Tafuri et al. 2023): plants: $\Delta^{13}C_{protein\text{-}bulk}$=–2‰, $\Delta^{13}C_{carbohydrates\text{-}bulk}$=+0.5‰, $\Delta^{15}N_{protein\text{-}bulk}$=0‰; terrestrial animals: $\Delta^{13}C_{protein\text{-}collagen}$= –2‰, $\Delta^{13}C_{lipids\text{-}collagen}$= -8‰, $\Delta^{15}N_{protein\text{-}collagen}$=0‰; aquatic animals: $\Delta^{13}C_{protein\text{-}collagen}$=–1‰, $\Delta^{13}C_{lipids\text{-}collagen}$=–7‰, $\Delta^{15}N_{protein\text{-}collagen}$=+1.5‰).

Macronutrient caloric concentration values were derived from Fernandes et al. (2015), but with uncertainty values doubled (Tafuri et al. 2023): plants (cereals): protein: 10±5%; lipids/carbohydrates 90±5%, terrestrial animals: protein: 30±5%; lipids/carbohydrates 70±5%, and fish (freshwater and marine): protein: 65±10%; lipids/carbohydrates 35±10%. Isotopic offsets between diet and human tissues, along with dietary routing mechanisms, were incorporated into the Bayesian mixing model. Bone collagen $\delta^{15}N$ was assumed to reflect dietary protein exclusively, with an isotopic offset of 5.5±0.5‰ (Fernandes et al. 2015). For bone collagen $\delta^{13}C$, an offset of 4.8±0.5‰ (Fernandes et al. 2012) was applied relative to food values. Additionally, we accounted for isotopic routing, with 74±4% of the signal originating from dietary protein and 26±4% from lipids and carbohydrates (Fernandes et al. 2012).

Table 4. Food source isotope values used in the ReSources analysis. Average isotopic values for the food groups are derived from Leggett et al. (2021). These do not include corrections for offsets between edible tissues and food remains; the corrected values are given in Table 5.

Food source	$\delta^{13}C$	sd	$\delta^{15}N$	sd
Terrestrial vegetation	−23.0	0.6	2.7	1.6
Terrestrial protein	−21.5	1.6	6.1	1.8
Marine fish	−13.4	1.1	15.0	1.7
Freshwater fish	−23.6	2.5	12.0	3.3

Table 5. Corrected isotopic food macronutrient values.

	$\delta^{13}C$ collagen (protein)	$\delta^{13}C$ collagen (lipids/carbohydrates)	$\delta^{15}N$ (protein)
Terrestrial vegetation	−25.0±1.0	−22.5±2.0	2.7±2.0
Terrestrial protein	−23.5±2.0	−29.5±2.0	6.1±2.0
Marine fish	−14.4±1.5	−20.4±1.5	15.0.0±2.0
Freshwater fish	−24.6±2.5	−30.6±2.5	12.0±3.5

Results

The range in human $\delta^{13}C$ values is relatively narrow, falling between −21.0‰ and−19.4‰. Variability in $\delta^{15}N$ values was higher, ranging from 9.5–12.8‰ (Table 3).

Figure 3 shows the Bayesian estimates for the caloric contributions from terrestrial plants and animal products, marine and freshwater fish. All estimates show that diet was dominated by caloric contributions from terrestrial animals and vegetation (cereals) although the 95% credible intervals for the estimates have a wide range, reflecting the uncertainty in food values (Table 6).

Freshwater fish is estimated to make up a small caloric contribution, although the 95% credible intervals for the estimates have an exceedingly wide range. Marine fish is estimated to make up a minimal, and possibly non-existent caloric contribution.

Reservoir effects occur when the carbon that is incorporated into a sample during life is not in equilibrium with the contemporary atmosphere. This gives the sample an apparent radiocarbon age older than that of a contemporary terrestrial sample (Bayliss and Marshall 2022, §1.6). To obtain an accurate calibrated date for such a sample, it is necessary to correct the apparent age during the calibration process using the relevant reservoir offset. But, given the lack of all-embracing research on freshwater offsets in England (Keaveney and Reimer 2012, table 1) and the wide ranges of the 95% credible intervals for the freshwater fish estimates we have chosen to employ a fully terrestrial calibration curve for radiocarbon calibration.

Table 6. Results for the ReSources source proportional mixing model: calorific contribution (%). (TV= terrestrial vegetation (cereals); TP= terrestrial protein, MF= marine fish; FF= freshwater fish)

Burial	Food	Mean	SD
123	TV	40	36.8
	TP	46.7	37.9
	MF	2	3.4
	FF	11.3	21.1
141	TV	26.1	33.5
	TP	60.7	37.7
	MF	1	2.6
	FF	12.1	24.2
166	TV	49	38.9
	TP	42	38.4
	MF	1.1	2.3
	FF	7.9	18.1
168	TV	28.3	33.7
	TP	58.4	37.6
	MF	1	2.2
	FF	12.3	22.6
174	TV	32.4	35.8
	TP	53.9	38.1
	MF	1.1	2.3
	FF	12.6	23
193	TV	31.1	34.7
	TP	54	37.9
	MF	1.3	2.4
	FF	13.6	22.9
196	TV	28	34.1
	TP	57.2	38.1
	MF	1.3	2.7
	FF	13.5	25
202	TV	33.6	36.1
	TP	52.8	38.5

Burial	Food	Mean	SD
	MF	1.2	2.5
	FF	12.4	23.2
218	TV	53	39.4
	TP	39.9	38.8
	MF	0.8	1.8
	FF	6.3	15.8
256	TV	61.1	38.7
	TP	33.1	37.4
	MF	0.6	1.7
	FF	5.1	14.6
267	TV	46.5	38
	TP	43.2	38
	MF	1.4	2.8
	FF	8.9	18.5
281	TV	42.8	39.1
	TP	48.8	39.3
	MF	0.7	1.6
	FF	7.6	18.2
294	TV	24.9	31.7
	TP	57.7	37.1
	MF	1.8	3.8
	FF	15.7	24.8
296	TV	41.6	37.7
	TP	48.2	38.3
	MF	1.4	2.8
	FF	8.8	18
300	TV	50.6	40.4
	TP	42.7	40.1
	MF	0.6	1.5
	FF	6.1	16.9
303	TV	35.4	37.9
	TP	53.1	39.7
	MF	1	2.7
	FF	10.5	22.9
306	TV	29	34.6
	TP	56.8	38.3
	MF	1.1	2.7
	FF	13.1	23.6
307	TV	30.6	33.5
	TP	50.2	37.6

Burial	Food	Mean	SD
	MF	2.9	4.6
	FF	16.3	24
353	TV	36.5	36.8
	TP	50.2	39
	MF	1.1	2.3
	FF	12.1	22.2
360	TV	37.4	39.2
	TP	53	40.3
	MF	0.7	1.6
	FF	8.9	21.6
361	TV	42.9	38.7
	TP	46.5	39.3
	MF	1	2
	FF	9.7	20.8
363	TV	51.4	39.5
	TP	41.2	39.2
	MF	0.7	1.6
	FF	6.7	16.7

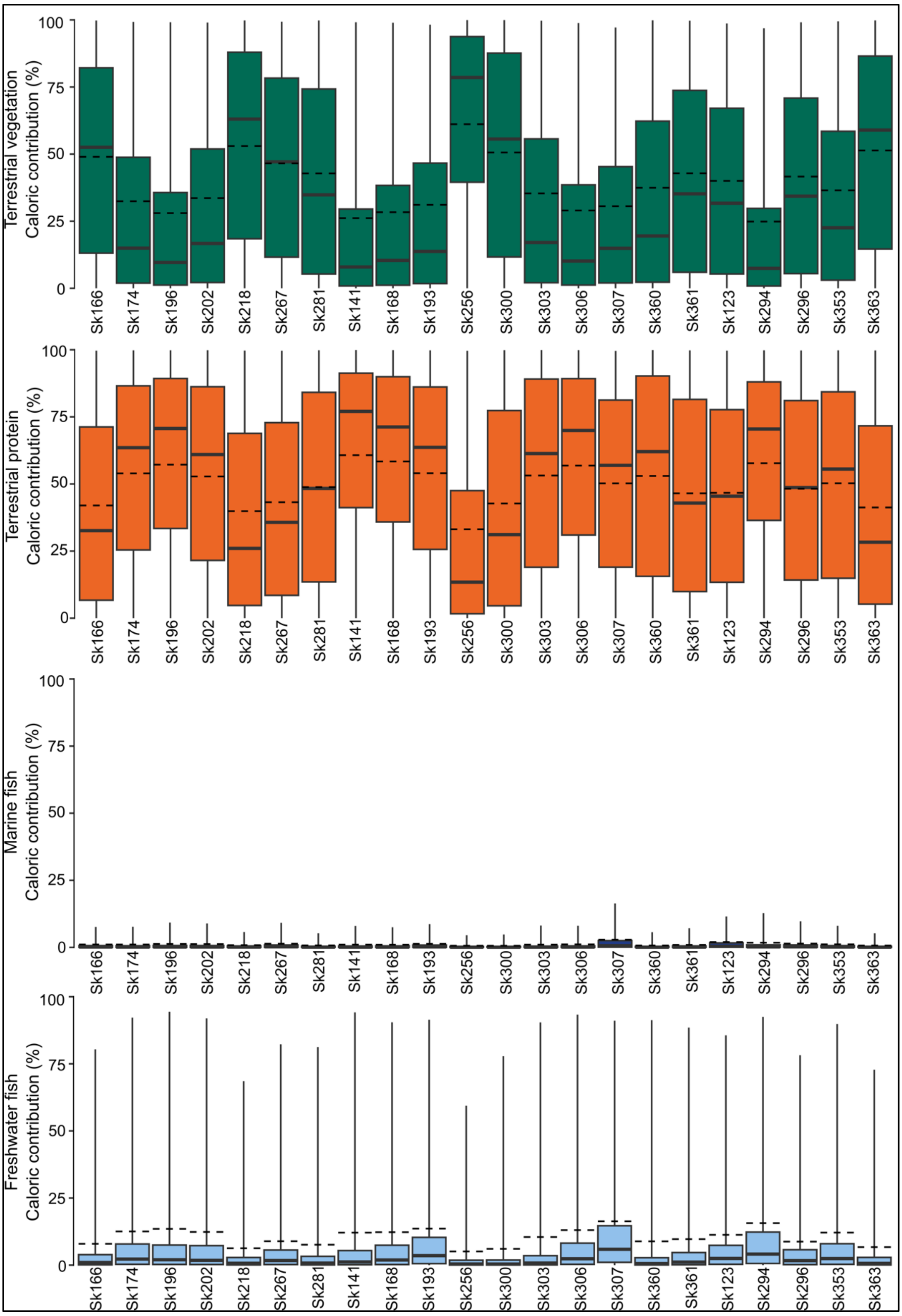

Figure 3. Bayesian caloric estimates for St Michael’s Church radiocarbon dated humans. Boxes represent a 68% credible interval (corresponding to the 16th and 84th percentiles), while the whiskers represent a 95% credible interval (corresponding to the 2.5th and 97.5th percentiles). The horizontal continuous line represents the estimated median (50th percentile).

Chronological Modelling

The chronological modelling presented here has been undertaken using OxCal 4.4 (Bronk Ramsey 2009), and the internationally agreed calibration curve for the northern hemisphere (IntCal20; Reimer et al. 2020). The model is defined by the OxCal CQL2 keywords and by the brackets on the left-hand side of Figures 4–7. The CQL2 code for the model is provided in the Appendix. In the figures, calibrated radiocarbon dates are shown in outline, and the posterior density estimates produced by the chronological modelling are shown in solid black. The other distributions correspond to aspects of the model. For example, the distribution '*StartPhase3b*' (Fig. 4) is the posterior density estimate for the date when Phase 3b burials commenced. In the text and tables highest posterior density intervals, which describe the posterior distributions, are given in italics have been rounded as outlined in Bayliss and Marshall (2022, §1.5).

The samples and the structure of the model

The model (Figs 4–7) estimates the chronologies of the burials in each of the three identified phases using uniform prior distributions for the spread of burial activity in each phase (Buck et al. 1992).

Phase 2b burials

In total, 39 graves, containing the remains of 40 individuals, were assigned to Phase 2b (Fig. 8). Most of the Phase 2b graves were in a strip, roughly 3–5m wide running north-east–south-west across the site. The distribution was almost certainly influenced by the Phase 1 ditch, within which some of the burials had been laid. Seven inhumations were sampled from Phase 2b graves (G166, G174, G196, G202, G218, G267 and G281; Table 3).

There was very little intercutting amongst the graves from this phase with only one sequence incorporated into the model (Fig. 9). G166 (OxA-X-2581-42) had been dug through an earlier grave (G167) that, although not dated, had cut an even earlier grave (G174). The sample from G166 (OxA-X-2581-42) had a proportionally quite low collagen yield (<1%) but, since the analytical parameters ($\delta^{13}C$, $\delta^{15}N$, and C:N) are within acceptable ranges (DeNiro 1985; Hoke et al. 2019; van Klinken 1999) the measurement has been included in the chronological model. The three radiocarbon measurements (SUERC-49794 and OxA-29265–6) on samples from SK174 are statistically consistent (T'=1.6; v=2; T′(5%)=6.0; Ward and Wilson 1978) and a weighted mean (G174; 1284±16 BP) was taken prior to calibration as providing the best estimate for the radiocarbon age of the individual.

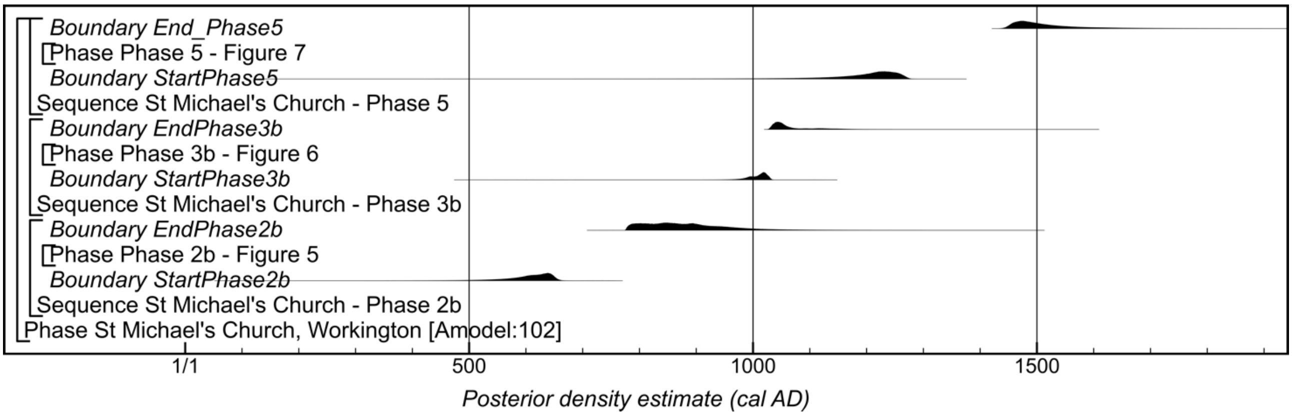

Figure 4. Probability distributions of dates from St Michael's Church, Workington. Each distribution represents the relative probability that an event occurs at a particular time. For each of the dates two distributions have been plotted: one in outline, which is the result of simple radiocarbon calibration, and a solid one, based on the chronological model used. Distributions other than those relating to particular samples correspond to aspects of the model. For example, the distribution '*StartPhase3b*' is the estimated date when Phase 3b burials commenced. The large square brackets down the left-hand side along with the OxCal keywords define the overall model exactly.

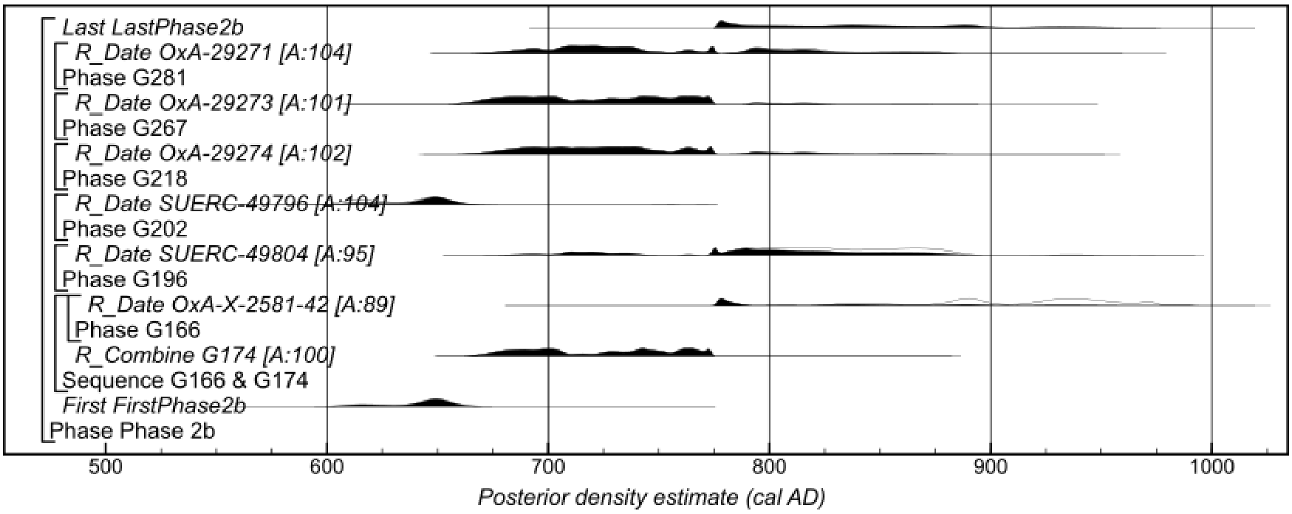

Figure 5. Probability distributions of dates from burial Phase 2b. The overall structure of the model is shown in Figure 4 and its other components in Figures 6 and 7.

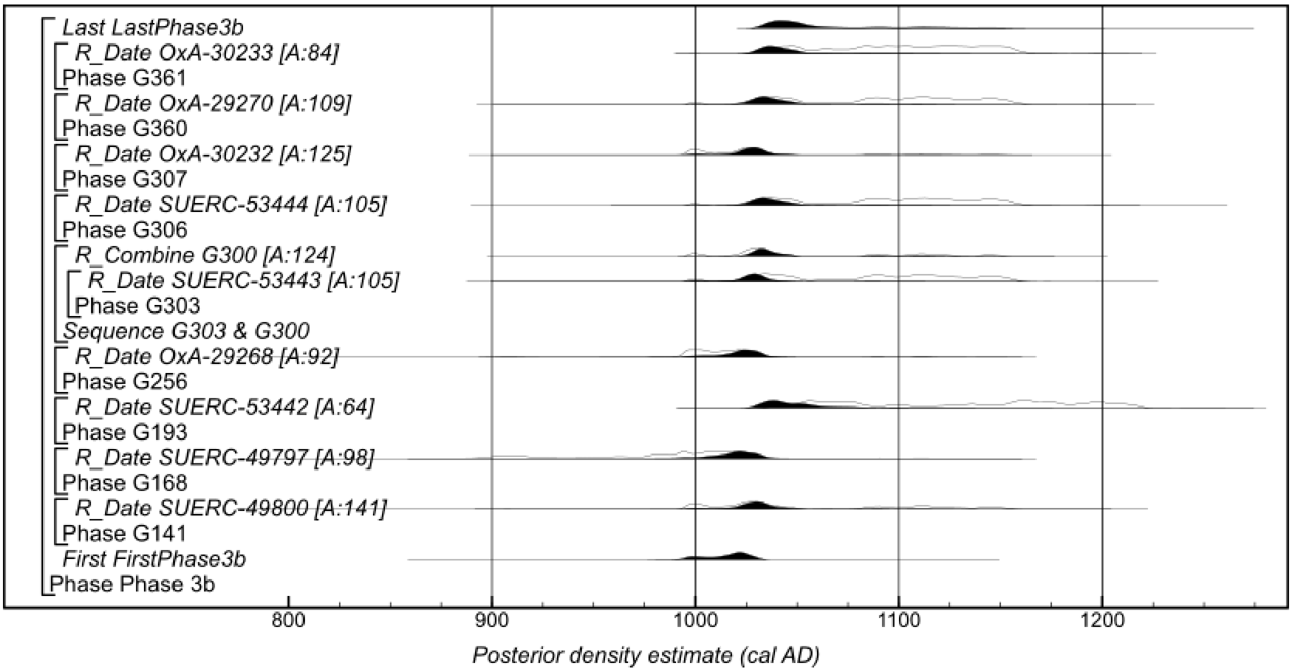

Figure 6. Probability distributions of dates from burial Phase 3b. The overall structure of the model is shown in Figure 4 and its other components in Figures 5 and 7.

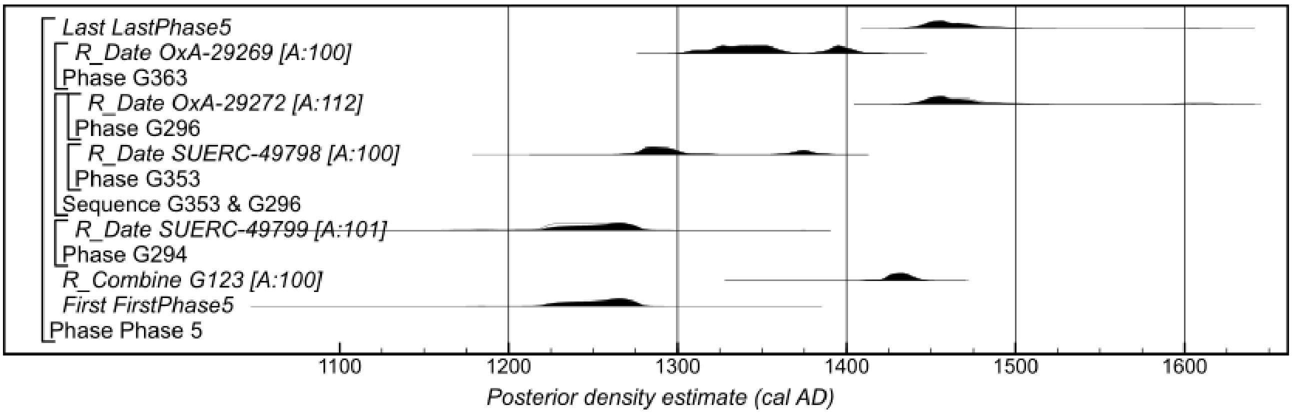

Figure 7. Probability distributions of dates from burial Phase 5. The overall structure of the model is shown in Figure 4 and its other components in Figures 5 and 6.

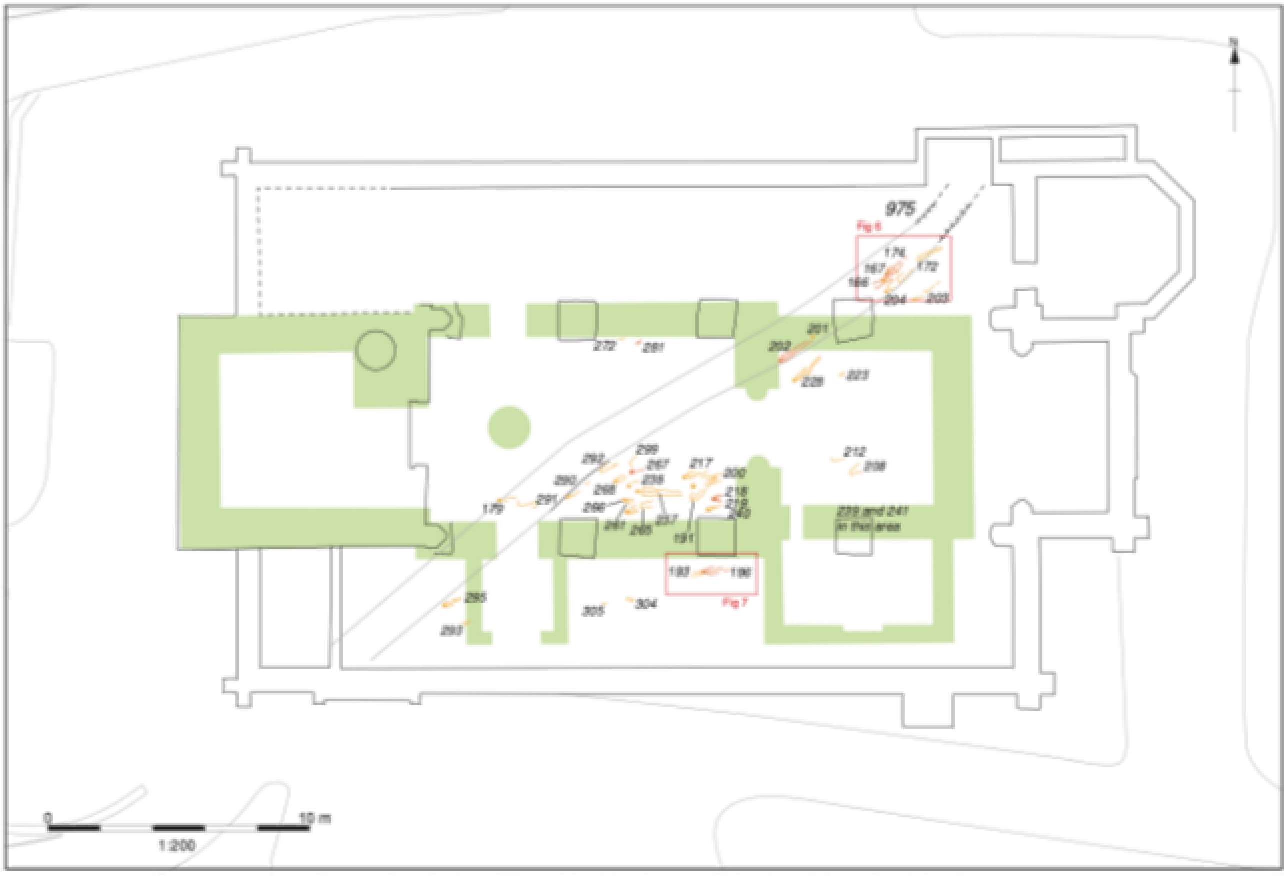

Figure 8. Phase 2b burials. [© Oxford Archaeology]

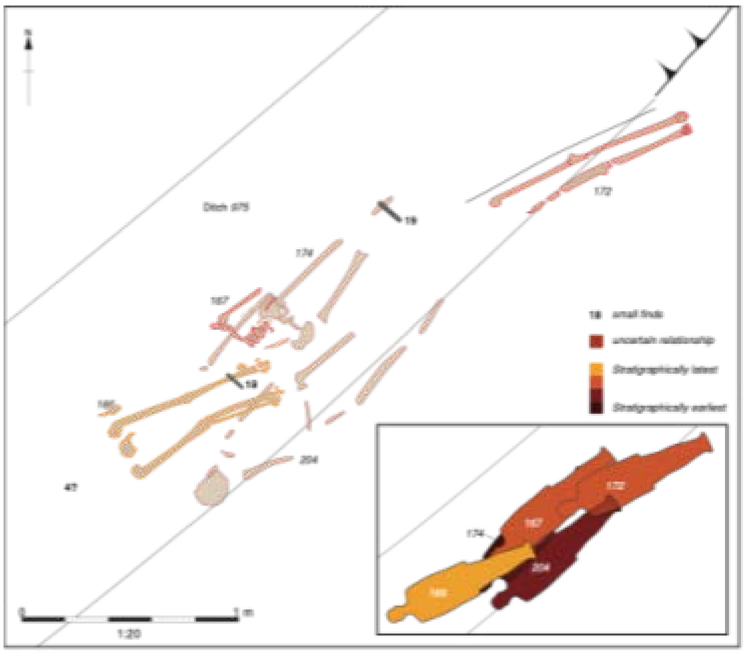

Figure 9. Intercutting Phase 2b graves 166, 167, 172 and 174. [© Oxford Archaeology]

Phase 3b burials

Phase 3b comprises a group of 18 burials in 16 graves (Fig. 10). This group was initially thought to be contemporary with the early Norman stone church, but a reconsideration of the stratigraphic evidence found that one of the graves was cut by its south wall (Zant and Parsons 2019, 23). It is plausible that the graves were spatially connected to an unrecorded church, possibly constructed entirely of timber.

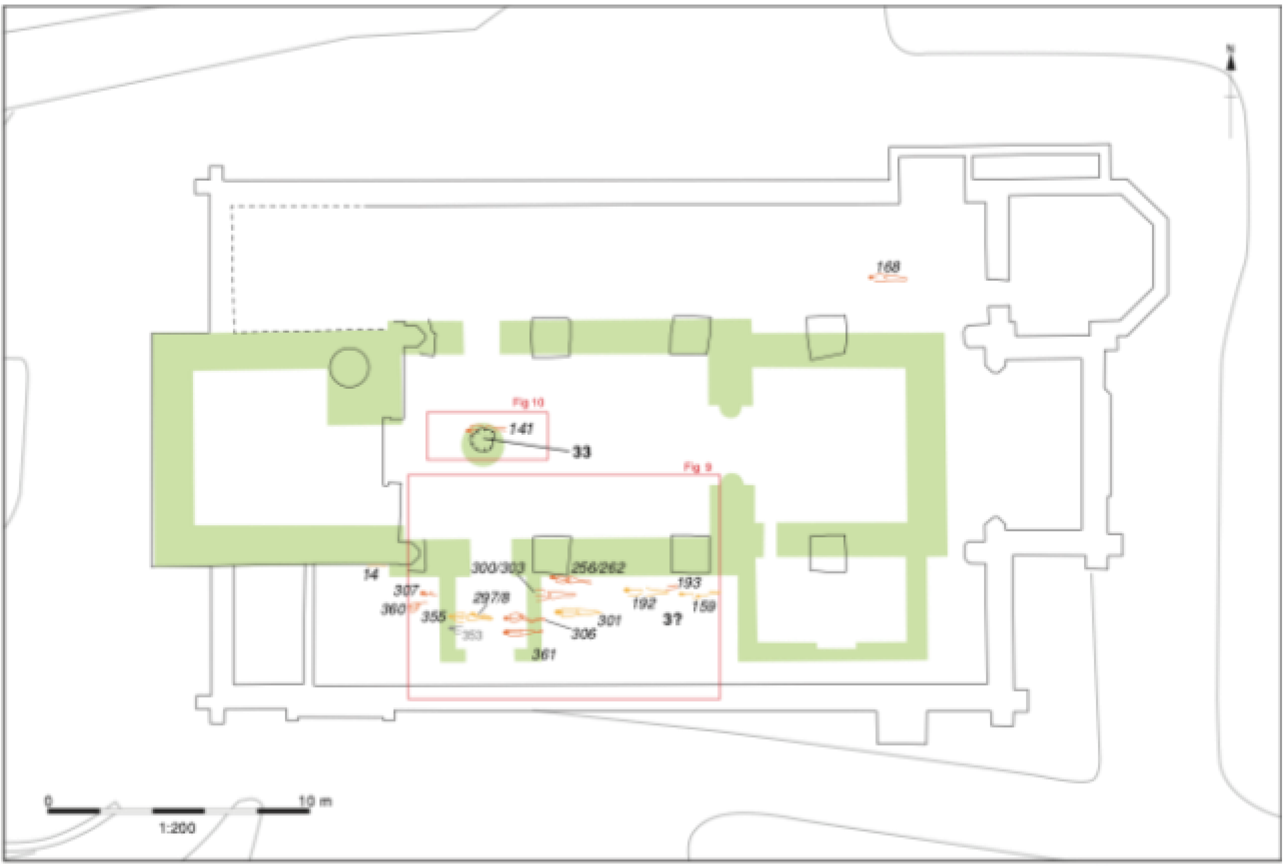

Figure 10. Phase 3b burials. [© Oxford Archaeology]

The main feature of the Phase 3b burials was a cluster of ten graves, each marked by a stone-lined cist. Among these, eight (159, 192, 301, 306, 307, 355, 360 and 361) contained single individuals, while two (256/262 and 300/303) held pairs of bodies. All graves were located just outside the south wall of the medieval nave, with grave 256/262 being intersected by the foundation (Fig. 11). The cists formed a distinct group within a narrow strip of ground, approximately 12.5m east-to-west and extending no more than 2.5m south of the nave wall. Since no similar burials were discovered elsewhere on the site and the cists did not appear to intercut, it is likely that these graves were roughly contemporary.

Figure 11. Phase 3b burials south of the later medieval church. [© Oxford Archaeology]

Ten inhumations (G141, G168, G193, G256, G300, G303, G306, G307, G360 and G361, G363; Table 2) including seven cist-graves lined (G256, G300, G303, G306, G307, G360, and G361; Zant and Parsons 2019, table 3) were dated.

Only a single sequence is incorporated into the model. Within the stone-lined cist, G303, located adjacent to the south wall of the nave of the church, the primary burial (G303; SUERC-53443) was overlain by a later burial (G300) from which statistically consistent radiocarbon measurements (OxA-29267 and SUERC-49795; T′=0.0; v=1; T′(5%)=3.8) have been combined (G300; 995±19 BP).

Phase 5 graves

Burial within the churchyard undoubtedly continued from the thirteenth century until the church's demolition and reconstruction in the early AD 1770s. However, only a limited selection of later medieval graves was analysed, and in some cases, radiocarbon dated, as the focus of the post-excavation project did not extend to the later development of the parish church. Most of the later medieval graves selected for analysis and dating were believed, based on limited stratigraphic evidence, to predate the addition of the south porch. Subsequent analysis, however, confirmed that only one of these graves was certainly earlier than the porch. Additionally, a few poorly stratified graves, chosen for their perceived similarity to dated pre-Norman burials (see below), were later determined through scientific dating to belong to the late medieval period.

A total of 25 later medieval burials, from 24 graves, were subjected to detailed recording and analysis. Of these, all but two were located on the south side of the nave (Fig. 12) and were thought, based on the limited stratigraphic evidence available, to certainly or possibly predate the construction of the south porch. The two exceptions (G123 and G130) were situated on the north side of the church, north of the chancel, and were notable for the placement of large cobbles on either side of the skull.

Radiocarbon results are available from five inhumations (G123, G294, G296, G353 and G363; Table 3) from Phase 5 burials. Statistically consistent radiocarbon measurements on samples from G123 (OxA-30378 and SUERC-53313; T′=0.2; v=1; T′(5%)=3.8) have been combined (G123; 486± 15BP) as providing the best estimate for the radiocarbon age of this individual.

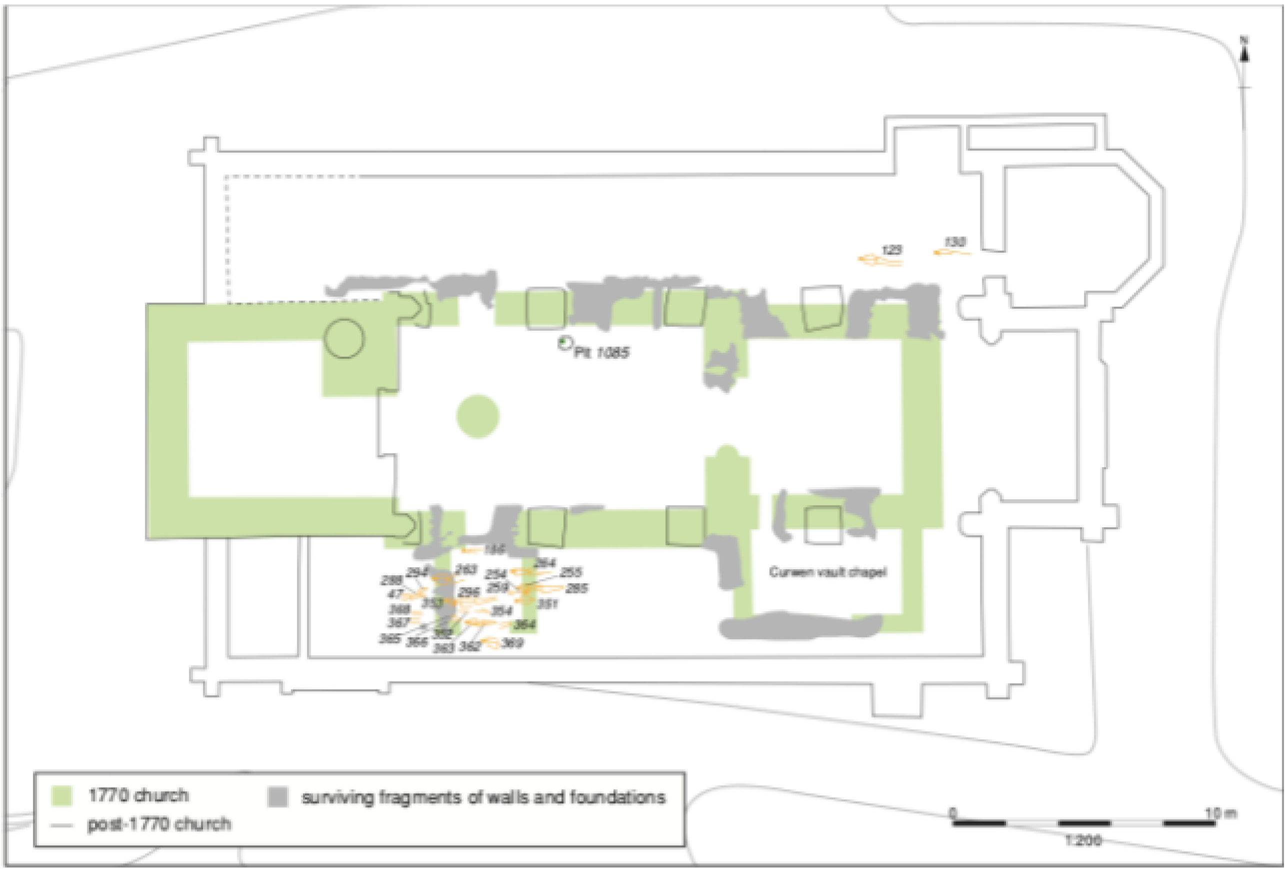

Figure 12. Phase 5 burials relative to the medieval church. [© Oxford Archaeology]

A narrative of burial at St Michael's Church

The model (Figs 4–7) shows good overall agreement (Amodel: 102) between the radiocarbon dates and the stratigraphic relationships between samples where these exist, and suggest that the earliest phase of burials (Phase 2b) started in *cal AD 470–665* (*95% probability*; *StartPhase2b*; Fig. 4), probably in *cal AD 585–655* (*68% probability)*. Phase 2b burials continued until *cal AD 775–1050* (*95% probability*; *EndPhase2b*; Fig. 4), probably until *cal AD 780–915* (*68% probability)*, in a period estimated to have lasted for *115–315 years* (*95% probability*; *phase_2b*; Fig. 13), probably for *125–245 years* (*68% probability).*

Phase 3b burials started in *cal AD 970–1035* (*95% probability*; *StartPhase3b*; Fig. 4), probably in *cal AD 990–1030* (*68% probability)*. Phase 3 burials continued until *cal AD 1028–1156* (*95% probability*; *EndPhase3b*; Fig. 4), probably until *cal AD 1031–1068* (*68% probability)*, in a period estimated to have lasted for *1–135 years* (*95% probability*; *Phase3b*; Fig. 13), probably for *1–52 years* (*68% probability).*

Phase 5 burials started in *cal AD 980–1280* (*95% probability*; *StartPhase5*; Fig. 4), probably in *cal AD 1173–1268* (*68% probability)*. Phase 5 burials continued until *cal AD 1439–1716* (*95% probability*; *EndPhase5*; Fig. 4), probably until *cal AD 1450–1539* (*68% probability)*, in a period estimated to have lasted for *166–259 years* (*95% probability*; *Phase5*; Fig. 13), probably for *182–228 years* (*68% probability).*

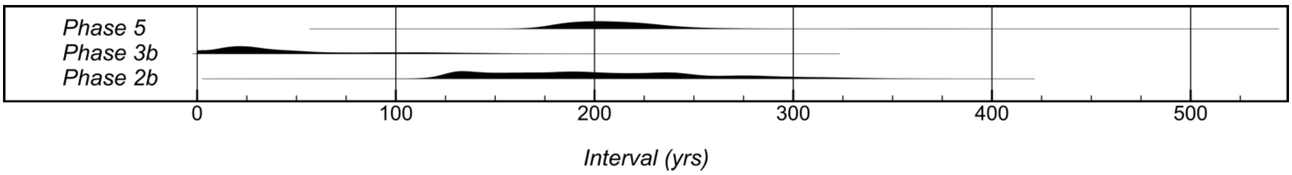

Figure 13. Summary of the number of years during which burial phases 2b, 3b and 5 were in use. The probabilities have been derived from the model shown in Figures 4–7.

The spatio-temporal development of burial at St Michael's Church

The dates when burial began and ended in the three dated phases at St Michael's Church are summarised in Figure 14 and Table 7.

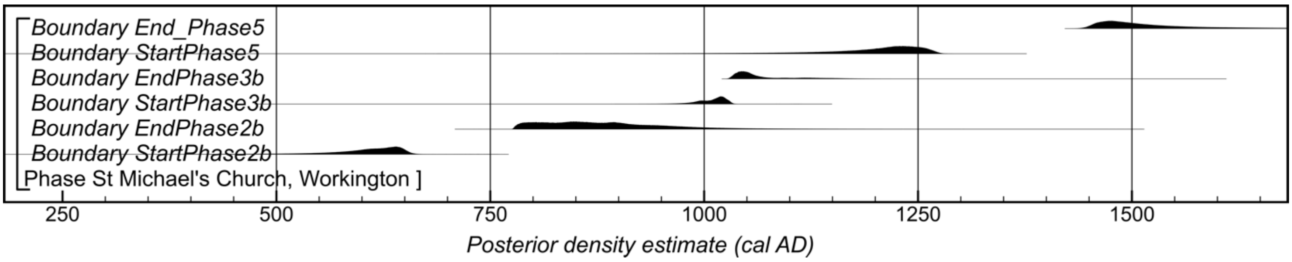

Figure 14. Summary of the posterior density estimates for the 'start' and 'end' of activity associated with burials from the three phases (2b, 3b and 5). The probabilities have been derived from the model shown in Figures 4–7.

Table 7. Highest Posterior Density intervals for the start and end of different phases of burial from St Michael's Church, from the model defined in Figures 4–7.

Parameter	*Posterior Density Estimate (95% probability)*	*Posterior Density Estimate (68% probability)*
StartPhase2b	*cal AD 470–665*	*cal AD 585–655*
EndPhase2b	*cal AD 775–1050*	*cal AD 780–915*
StartPhase3b	*cal AD 970–1035*	*cal AD 990–1030*
EndPhase3b	*cal AD 1028–1156*	*cal AD 1031–1068*
StartPhase5	*cal AD 980–1280*	*cal AD 1173–1268*
EndPhase5	*cal AD 1439–1716*	*cal AD 1450–1539*

Phase 2b graves were primarily concentrated in a 3–5m wide zone-oriented northeast–southwest across the site, situated southeast of the Phase 1 ditch [975]. The placement of these graves was likely influenced by the Phase 1 ditch, with some burials located within its bounds. Following a cessation in burial that is estimated to have lasted for *−40–250 years* (*95% probability*; *Phases 2b&3b*; distribution not shown), probably for *85–225 years* (*68% probability),* the more closely aligned east–west burials of Phase 3b began in the eleventh century cal AD. These dated burials provide a *terminus post quem* for the construction of the medieval church of *cal AD 1028–1156* (*94% probability*; *EndPhase3b*; Fig. 14), probably of *cal AD 1031–1068* (*68% probability*). Phase 3b burials took place for a restricted period probably lasting for only a few generations and were predominantly in an area where the south door of the church and its external porch were to be built subsequently.

Although the later medieval burials were not exclusively sampled as part of the radiocarbon dating programme, due to the number of them and difficulty of determining any spatial differentiation in their location — hence they are under-sampled in the model — Phase 5 burials started following an interval of *−105–240 years* (*95% probability*;

Phases 3b&5; distribution not shown), probably after an interval of *90–220 years* (*68% probability)* after the end of Phase 3b.

Cist-lined graves

One of the initial expectations was that there might be some chronological sensitivity to the cist-lined graves. The modeled probability densities for seven of the 11 cist-lined graves were extracted from the model and are shown in Figure 15. The dated cist-lined graves date from the second quarter of the eleventh century cal AD.

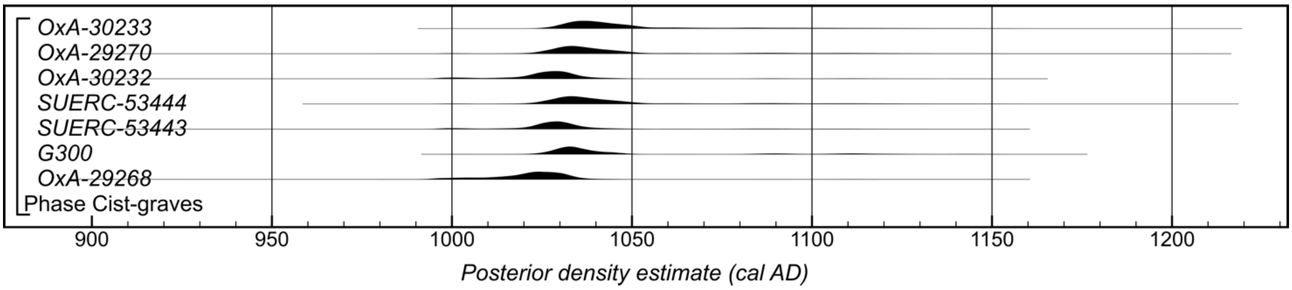

Figure 15. Posterior density estimates for burials in cist-lined graves. The probabilities have been derived from the model shown in Figures 4–7.

Discussion

The earliest pre-Norman burials (Phase 2b) in the cemetery were aligned broadly north-east to south-west (head to the south-west) and interred for one–two centuries most probably from *cal AD 585–655* (*68% probability*) to *cal AD 780–915* (*68% probability*). This contrasts with later burials, and the medieval and post-medieval churches, which were more truly aligned east-west.

The group of burials (Phase 3b) aligned more closely east–west, and primarily pre-dating the construction of the medieval church, date from the first half of the eleventh century cal AD (Fig. 15). The excavations also found a significant assemblage of mid- to later tenth-century stone sculpture, including cross shafts and hogback fragments, decorated with Scandinavian Borre- and Jellinge-style artwork. Probably, therefore, these burials formed part of a cemetery at an ecclesiastical establishment associated with this sculpture, though no trace of buildings or any other features that may have formed part of this was found.

Construction of the medieval church would have taken place sometime after the end of Phase 3b dated to *cal AD 1028–1156* (*95% probability*; *EndPhase3b;* Fig. 15), probably to *cal AD 1031–1068* (*68% probability*).

References

Bayliss, A. and Marshall, P. 2022 *Radiocarbon Dating and Chronological Modelling: Guidelines and Best Practice* (Liverpool)

Bayliss, A., Marshall, P., Dee, M., Friedrich, M., Heaton, T., and Wacker, L. 2020 **‘**IntCal20 tree-rings: an archaeological SWOT analysis’, *Radiocarbon,* 62, 1045–78. https://doi.org/10.1017/RDC.2020.77

Brock, F., Higham, T., and Bronk Ramsey, C. 2010 ‘Pre-screening techniques for identification of samples suitable for radiocarbon dating of poorly preserved bones’, *Journal of Archaeological Science*, 37, 855–65. https://doi.org/10.1016/j.jas.2009.11.015

Bronk Ramsey, C. 2009 'Bayesian analysis of radiocarbon dates', *Radiocarbon,* 51(1), 337–60. https://doi.org/10.1017/S0033822200033865

Bronk Ramsey, C., Higham, T., Bowles, A., and Hedges, R. E. M. 2004a ‘Improvements to the pre-treatment of bone at Oxford’, *Radiocarbon*, 46, 155–63. https://doi.org/10.1017/S0033822200039473

Bronk Ramsey, C., Higham, T., and Leach, P. 2004b ‘Towards high-precision AMS: progress and limitations’, *Radiocarbon,* 46(1), 17–24. https://doi.org/10.1017/S0033822200039308

Buck, C. E., Litton, C. D., Smith, A. F. M. 1992 ‘Calibration of radiocarbon results pertaining to related archaeological events’, Journal of Archaeological Science, 19 (5), 497–512. https://doi.org/10.1016/0305-4403(92)90025-X

Collins, M. J., Nielsen-Marsh, C. M., Hiller, J., Smith, C. I., Roberts, J. P., Progodich, R. V., Wess, T. J., Csapò, J., Millard, A. R., and Turner-Walker, G. 2002 ‘The survival of organic matter in bone: a review’, *Archaeometry*, 44, 383–94. https://doi.org/10.1111/1475-4754.t01-1-00071

Dee, M. and Bronk Ramsey, C. 2000 ‘Refinement of graphite target production at ORAU’, *Nuclear Instruments and Methods in Physics Research B: Section B: Beam Interactions with Materials and Atoms,* 172, 449–53. https://doi.org/10.1016/S0168-583X(00)00337-2

DeNiro, M. 1985 ‘Postmortem preservation and alteration of *in vivo* bone collagen isotope ratios in relation to palaeodietary reconstruction’, *Nature*, 317, 806–9. https://doi.org/10.1038/317806a0

Dunbar, E., Cook, G. T., Naysmith, P., Tipney, B. G., and Xu, S. 2016 'AMS ^{14}C dating at the Scottish Universities Environmental Research Centre (SUERC) Radiocarbon Dating Laboratory', *Radiocarbon,* 58(1), 9–23. https://doi.org/10.1017/RDC.2015.2

Fernandes, R. 2016 'A simple(R) model to predict the source of dietary carbon in individual consumers', *Archaeometry*, 58(3), 500–12. https://doi.org/10.1111/arcm.12193

Fernandes, R., Nadeau, M.-J. and Grootes, P. M. 2012 'Macronutrient-based model for dietary carbon routing in bone collagen and bioapatite', *Archaeological and Anthropological Sciences*, 4, 291–301. https://doi.org/10.1007/s12520-012-0102-7

Fernandes, R., Millard, A. R., Brabeck, M., Nadeau, M-J., and Grootes, P. 2014 'Food Reconstruction Using Isotopic Transferred Signals (FRUITS): a Bayesian model for diet reconstruction', *PLoS ONE*, 9. https://doi.org/10.1371/journal.pone.0087436

Fernandes, R., Grootes, P., Nadeau M.-J., and Nehlich, O. 2015 'Quantitative diet reconstruction of a Neolithic population using a Bayesian mixing model (FRUITS): the case study of Ostorf (Germany)', *American Journal of Physical Anthropology*, 158, 325–40. https://doi.org/10.1002/ajpa.22788

Freeman, S. P. H. T., Cook, G. T., Dougans, A. B., Naysmith, P., Wilcken, K. M., and Xu, S. 2010 'Improved SSAMS performance', *Nuclear Instruments and Methods in Physics Research B: Section B: Beam Interactions with Materials and Atoms*, 268–7/8, 715–17. https://doi.org/10.1016/j.nimb.2009.10.012

Gross, M. and Fernandes, R. 2024 *ReSources: Food Reconstruction Using Isotopic Transferred Signals*. R package version 24.11.0, https://pandora-isomemo.github.io/ReSources/

Heaton, T., Vogel, J., von la Chevallerie, G., and Collett, G. 1986 'Climatic influence on the isotopic composition of bone nitrogen', *Nature*, 322, 822–3. https://doi.org/10.1038/322822a0

Hedges, R. E. M., Humm, M. J., Foreman, J., Klinken, G. J. van, and Bronk, C. R. 1992 'Developments in sample combustion to carbon dioxide, and in the Oxford AMS carbon dioxide ion source system', *Radiocarbon*, 34, 306–11. https://doi.org/10.1017/S0033822200063463

Hoke, N., Rott, A., Johler, S., Reul, A., Beck, A., Günther, A., Hochleitner, R., Kaliwoda, M., and Harbeck, M. 2019 'How bone degradation, age, and collagen extraction methods affect stable isotope analysis', *Archaeological and Anthropological Sciences,* 11, 3357–74. https://doi.org/10.1007/s12520-018-0765-9

Keaveney, E. M., and Reimer, P. J. 2012 'Understanding the variability in freshwater radiocarbon reservoir offsets: a cautionary tale', *Journal of Archaeological Science,* 39, 1306–16. https://doi.org/10.1016/j.jas.2011.12.025

Leggett, S., Rose, A., Praet, E., and Le Roux, P. 2021 'Multi-tissue and multi-isotope ($\delta^{13}C$, $\delta^{15}N$, $\delta^{18}O$ and $^{87/86}Sr$) data for early medieval human and animal palaeoecology', *Ecology,* 102, e03349. https://doi.org/10.1002/ecy.3349

Longin, R. 1971 'New method of collagen extraction for radiocarbon dating', *Nature*, 230, 241–2. https://doi.org/10.1038/230241a0

Marshall, P., Bronk Ramsey, C., Dunbar, E., and Zant, J. 2019 'Radiocarbon dating and stable isotope analysis', in J. Zant and A. Parsons *St Michael's Church, Workington. Excavation of an Early Medieval Cemetery* (Lancaster) 107–18

Müldner, G., and Richards, M. P. 2005 'Fast or feast: reconstructing diet in later medieval England by stable isotope analysis', *Journal of Archaeological Science*, 32, 39–48. https://doi.org/10.1016/j.jas.2004.05.007

Naysmith, P., Cook, G. T., Freeman, S. P. H. T., Scott, E. M., Anderson, R., Xu, S., Dunbar, E., Muir, G. K. P., Dougans, A., Wilcken, K., Schnabel, C., Russell, N., Ascough, P. L., and Maden, C. 2010 '^{14}C AMS at SUERC: improving QA data with the 5MV Tandem and 250 kV SSAMS', *Radiocarbon*, 52, 263–71. https://doi.org/10.1017/S003382220004529X

Peterson, B. J. and Fry, B. 1987 'Stable isotopes in ecosystem studies', *Annual Review of Ecology, Evolution, and Systematics,* 18, 293–320. https://doi.org/10.1146/annurev.es.18.110187.001453

Reimer, P. J., Bard, E., Bayliss, A., Beck, J. W., Blackwell, P., Bronk Ramsey, C., Buck, C. E., Cheng, H., Edwards, R. L., Friedrich, M., Grootes, P. M., Guilderson, T. P., Haflidason, H., Hajdas, I., Hatté, C., Heaton, T. J., Hoffmann, D. L., Hogg, A. G., Hughen, K. A., Kaiser, K. F., Kromer, B., Manning, S. W., Niu, M., Reimer, R. W., Richards, D. A., Scott, E. M., Southon, J. R., Staff, R. A., Turney, C. S. M., and van der Plicht, J., 2013 'IntCal13 and Marine13 radiocarbon age calibration curves 0–50,000 years cal BP', *Radiocarbon*, 55, 1869–87. https://doi.org/10.2458/azu_js_rc.55.16947

Reimer, P. J., Austin, W. E. N., Bard, E., Bayliss, A., Blackwell, P. G., Bronk Ramsey, C., Butzin, M., Cheng, H., Edwards, R. L., Friedrich, M., Grootes, P. M., Guilderson, T. P., Hajdas, I., Heaton, T. J., Hogg, A. G., Hughen, K. A., Kromer, B., Manning, S. W., Muscheler, R., Palmer, J. G., Pearson, C., Van Der Plicht, J., Reimer, R. W., Richards, D.

A., Scott, E. M., Southon, J. R., Turney, C. S. M., Wacker, L., Adolphi, F., Büntgen, U., Capano, M., Fahrni, S. M., Fogtmann-Schulz, A., Friedrich, R., Köhler, P., Kudsk, S., Miyake, F., Olsen, J., Reinig, F., Sakamoto, M., Sookdeo, A. and Talamo, S. 2020 'The IntCal20 northern hemisphere radiocarbon age calibration curve (0–55 cal kBP)', *Radiocarbon,* 64(2), 725–57. https://doi.org/10.1017/RDC.2020.41

Scott, E.M., Naysmith P.,and Cook G.T. 2017 'Should archaeologists care about ^{14}C intercomparisons? Why? A summary report on SIRI', *Radiocarbon,* 59, 1589–96. https://doi.org/10.1017/RDC.2017.12

Slota Jr, P. J., Jull, A. J. T., Linick, T. W., and Toolin, L. J. 1987 'Preparation of small samples for ^{14}C accelerator targets by catalytic reduction of CO', *Radiocarbon*, 29, 303–6. https://doi.org/10.1017/S0033822200056988

Soncin, S., Talbot, H. M., Fernandes, R., Harris, A. J., von Tersch, M., Robson, H. K., Bakker, J. K., Richter, K. K., Alexander, M. M., Ellis, S. P., Thompson, G., Amoretti, V., Osanna, M., Caso, M., Sirano, F., Fattore, L., Colonese, A. C., Garnsey, P. D., Bondioli, L., and Craig, O. E. 2021 'High-resolution dietary reconstruction of victims of the 79 CE Vesuvius eruption at Herculaneum by compound-specific isotope analysis', *Science Advances*, 7, eabg5791. https://doi.org/10.1126/sciadv.abg5791

Stuiver, M. and Polach, H. A. 1977 'Discussion reporting of ^{14}C data', *Radiocarbon,* 19(3), 355–63: https://doi.org/10.1017/S0033822200003672

Tafuri M.A, Soncin S, Panella S, Thompson JE, Tiberi I, Fabbri PF, Sivilli S, Radina F, Minozzi S, Muntoni IM, Fiorentino G, Robb J. 2023 'Regional long-term analysis of dietary isotopes in Neolithic southeastern Italy: new patterns and research directions', *Scientific Reports*, 13(1):7914. https://doi.org/10.1038/s41598-023-34771-y

van Klinken, G. J. 1999 'Bone collagen quality indicators for palaeodietary and radiocarbon measurements', *Journal of Archaeological Science,* 26, 687–95. https://doi.org/10.1006/jasc.1998.0385

Vandeputte, K., Moens, L., and Dams, R. 1996 'Improved sealed-tube combustion of organic samples to CO_2 for stable isotopic analysis, radiocarbon dating and percent carbon determinations', *Analytical Letters*, 29, 2761–73. https://doi.org/10.1080/00032719608002279

Ward, G. K., and Wilson, S. R. 1978 'Procedures for comparing and combining radiocarbon age determinations: a critique', *Archaeometry,* 20(1), 19–32. https://doi.org/10.1111/j.1475-4754.1978.tb00208.x

Zant, J., and Parsons, A. 2019 *St Michael's Church, Workington. Excavation of an Early Medieval Cemetery* (Lancaster)

Appendix

CQL2 code for the chronological model shown in Figures 4–7

```
Options()
 {
  Resolution=1;
  kIterations=20000;
 };
 Plot()
 {
  Phase("St Michael's Church, Workington")
  {
   Sequence("St Michael's Church - Phase 2b")
   {
    Boundary("StartPhase2b");
    Phase("Phase 2b")
    {
     First("FirstPhase2b");
     Sequence("G166 & G174")
     {
      R_Combine("G174")
      {
       R_Date("SUERC-49794", 1275, 26);
       R_Date("OxA-29265", 1312, 27);
       R_Date("OxA-29266", 1268, 26);
      };
      Phase("G166")
      {
       R_Date("OxA-X-2581-42", 1150, 23);
      };
     };
     Phase("G196")
     {
      R_Date("SUERC-49804", 1213, 28);
     };
     Phase("G202")
     {
      R_Date("SUERC-49796", 1407, 26);
     };
     Phase("G218")
     {
      R_Date("OxA-29274", 1268, 26);
     };
     Phase("G267")
```

```
  {
   R_Date("OxA-29273", 1287, 26);
  };
  Phase("G281")
  {
   R_Date("OxA-29271", 1248, 26);
  };
  Last("LastPhase2b");
  Span("Phase2b");
 };
 Boundary("EndPhase2b");
};
Sequence("St Michael's Church - Phase 3b")
{
 Boundary("StartPhase3b");
 Phase("Phase 3b")
 {
  First("FirstPhase3b");
  Phase("G141")
  {
   R_Date("SUERC-49800", 1002, 30);
  };
  Phase("G168")
  {
   R_Date("SUERC-49797", 1057, 30);
  };
  Phase("G193")
  {
   R_Date("SUERC-53442", 903, 30);
  };
  Phase("G256")
  {
   R_Date("OxA-29268", 1030, 25);
  };
  Sequence("G303 & G300")
  {
   Phase("G303")
   {
    R_Date("SUERC-53443", 977, 30);
   };
   R_Combine("G300")
   {
    R_Date("SUERC-49795", 997, 26);
    R_Date("OxA-29267", 993, 27);
   };
```

```
  };
  Phase("G306")
  {
   R_Date("SUERC-53444", 969, 30);
  };
  Phase("G307")
  {
   R_Date("OxA-30232", 1008, 23);
  };
  Phase("G360")
  {
   R_Date("OxA-29270", 971, 27);
  };
  Phase("G361")
  {
   R_Date("OxA-30233", 948, 23);
  };
  Last("LastPhase3b");
  Span("Phase3b");
 };
 Boundary("EndPhase3b");
};
Sequence("St Michael's Church - Phase 5")
{
 Boundary("StartPhase5");
 Phase("Phase 5")
 {
  First("FirstPhase5");
  R_Combine("G123")
  {
   R_Date("OxA-30378", 478, 23);
   R_Date("SUERC-53313", 492, 19);
  };
  Phase("G294")
  {
   R_Date("SUERC-49799", 791, 30)
   {
   };
  };
  Sequence("G353 & G296")
  {
   Phase("G353")
   {
    R_Date("SUERC-49798", 698, 30);
   };
```

```
    Phase("G296")
    {
     R_Date("OxA-29272", 411, 24);
    };
   };
   Phase("G363")
   {
    R_Date("OxA-29269", 590, 25);
   };
   Last("LastPhase5");
   Span("Phase5");
  };
  Boundary("EndPhase5");
  Before()
  {
   C_Date(1950, 0);
  };
 };
};
```

Historic England

Historic England's Research Reports

We are the public body that helps people care for, enjoy and celebrate England's historic environment.

We carry out and fund applied research to support the protection and management of the historic environment. Our research programme is wide-ranging and both national and local in scope, with projects that highlight new discoveries and provide greater understanding, appreciation and enjoyment of our historic places.

More information on our research strategy and agenda is available at HistoricEngland.org.uk/research/agenda.

The Research Report Series replaces the former Centre for Archaeology Reports Series, the Archaeological Investigation Report Series, the Architectural Investigation Report Series, and the Research Department Report Series.

All reports are available at HistoricEngland.org.uk/research/results/reports. There are over 7,000 reports going back over 50 years. You can find out more about the scope of the Series here: HistoricEngland.org.uk/research/results/about-the-research-reports-database.

Keep in touch with our research through our digital magazine *Historic England Research* HistoricEngland.org.uk/whats-new/research.

ISSN 2398-3841 (Print)
ISSN 2059-4453 (Online)